Sixth International Symposium on Turbulence and Shear Flow Phenomena
Seoul, Korea, 22-24 June 2009

ANALYSIS OF WALL THERMOCHEMICAL ABLATION BY THE USE OF DIRECT SIMULATIONS OF TURBULENT PERIODIC CHANNEL FLOW

Olivier Cabrit
CERFACS, CFD Team
Toulouse, France
olivier.cabrit@cerfacs.fr

Franck Nicoud
Université Montpellier 2 and I3M
CNRS UMR 5149
Montpellier, France

ABSTRACT

This study presents the results obtained performing a set of direct numerical simulations (DNS) that aim at representing the behavior of a turbulent boundary layer over an isothermal wall subjected to thermochemical ablation. It is shown how the results can be analyzed focussing on species/momentum/energy/atom conservation.

INTRODUCTION

Ablative surface flows often arise when using thermal protection materials for preserving structural components of atmospheric re-entry spacecrafts (Zhong *et al.*, 2008) and Solid Rocket Motors (SRM) internal insulation or nozzle assembly (Koo *et al.*, 2006). In the latter application, carbon-carbon composites are widely used and exposed to severe thermochemical attack. The nozzle surface recedes due to the action of oxidizing species, typically H_2O and CO_2, which is an issue during motor firing since the SRM performance is lowered by the throat area increase and the apparition of surface roughness. Full-scale motor firings are very expensive and do not provide sufficient information to understand the whole phenomenon. Numerical simulations can then be used to generate precise and detailed data set of generic turbulent flows under realistic operating conditions.

Many studies have already proposed to couple numerically the gaseous phase and the solid structure (Keswani and Kuo, 1983; Baiocco and Bellomi, 1996; Kendall *et al.*, 1967). However, most of them are dedicated to the structural material characterization by predicting the recession rate or the surface temperature and few are dealing with the fluid characterization. Hence, the objective of the present study is to increase the understanding of changes of the turbulent boundary layer (TBL) when thermochemical ablation occurs. In this framework, the present study aims at presenting the results obtained from a set of DNS of turbulent reacting multicomponent channel flow with isothermal ablative walls. Another simulation led under the same operating conditions but with inert walls will constitute a reference case. Results of the preliminary study (Cabrit *et al.*, 2007) have been improved thanks to an ensemble average procedure giving more convergence for analyzing the mass/momentum/energy conservations.

The full 3D compressible reacting Navier-Stokes equations are solved by using the AVBP code (see http://www.cerfacs.fr/cfd/publications.php) developed at CERFACS. This third-order accurate solver (in both space and time) is dedicated to LES/DNS of reacting flows and has been widely used and validated during the past years (Schmitt *et al.*, 2007; Mendez and Nicoud, 2008).

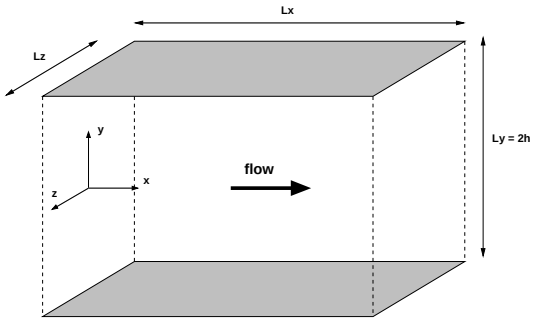

DNS	Re_τ	Lx/h	Lz/h	wall B.C.
Inert	300	3.2	1.25	isothermal/no-slip
	homogeneous directions: x, z, t			
ablation	300	3.2	1.25	isothermal/blowing
	homogeneous directions: x, z			

Figure 1: Computational domain.

The classical channel flow configuration (Kim *et al.*, 1987) is used in this study. As shown in Fig. 1, periodic boundary conditions are used in both streamwise and spanwise directions. A no-slip isothermal boundary condition is imposed for inert case while a blowing isothermal boundary condition is set for the ablation case (see below for its description). Moreover, the streamwise flow is enforced by adding a source term to the momentum conservation equation while a volume source term that warms the fluid is added to the energy conservation equation in order to sustain the mean temperature inside the computational domain.

Realistic gas ejected from SRM nozzles contains about a hundred gaseous species. Only the ones whose mole fraction is greater than 0.001 are kept to generate a simpler mixture, nitrogen being used as a dilutent. Hence, seven species are kept for the simulation: H_2, H, H_2O, OH, CO_2, CO and N_2. To simulate the chemical kinetics of this mixture, one applies a kinetic scheme based on seven chemical reactions extracted from the GRI-Mech elementary equations (see http://www.me.berkeley.edu/gri_mech).

For simplification reasons, the questions of two-phase flow effects, mechanical erosion and surface roughness are

not accounted for in the present work. Hence, inspired by the wall recession model proposed by Keswani and Kuo (Keswani and Kuo,1983) and the work of Kendall, Rindal and Bartlett (Kendall *et al.*, 1967) a reacting gaseous phase model is merely coupled with a boundary condition for thermochemically ablated walls. A full description of the boundary condition is given in Cabrit *et al.*, 2007. It is based on the mass budget of the species k at the solid surface:

$$\rho_w Y_{k,w} \left(V_{inj} + V_k\right) = \dot{s}_k \tag{1}$$

where subscript w refers to wall quantities, ρ_w denotes the density of the mixture, $Y_{k,w}$ the mass fraction of species k, V_{inj} the convective velocity of the mixture at the surface, V_k the diffusion velocity of k in the direction normal to the wall and $\dot{s}_k$ the production rate of k. One obtains the injection velocity (also called Stephan velocity) by summing over all the species:

$$V_{inj} = \frac{1}{\rho_w} \sum_k \dot{s}_k \tag{2}$$

Moreover, making use of the Hirschfelder and Curtiss approximation with correction velocity for diffusion velocities (Hirschfelder *et al.*, 1964), it is possible to relate $Y_{k,w}$ to its normal gradient at the solid/gas interface:

$$\begin{aligned}\nabla Y_{k,w} =& \frac{Y_{k,w}}{\mathcal{D}_k} \left(V_{inj} + V^{cor} + W_w \mathcal{D}_k \sum_l \frac{\nabla Y_{l,w}}{W_l} \right) \\ & - \frac{\dot{s}_k}{\rho_w \, \mathcal{D}_k}\end{aligned} \tag{3}$$

where $\mathcal{D}_k$ is the diffusion coefficient of k in the mixture, W_k the molecular weight of k, W_w the mean molecular weight of the mixture at the wall, $X_{k,w}$ the mole fraction of k and V^{cor} a correction diffusion velocity that ensures global mass conservation. The latter equation is used as a boundary condition for species k, Eq. (2) is used for the normal momentum equation (the tangential velocity is supposed null at the ablative wall), and the surface temperature is imposed. Note that because the production rate of species k depends on the concentration of the oxidizing species at the wall surface, the Stephan velocity is both space and time dependent which differs from the classical blowing surface DNS (Sumitani and Kasagi, 1995).

DESCRIPTION OF THE SIMULATIONS

We consider a flow at low Mach number ($M = 0.2$), whose mean volume temperature is sustained to $T_{\text{mean}} = 3000K$, and we set the wall temperature to $T_w = 2750K$. The source term enforcing the streamwise flow is set in order to impose a friction Reynolds $Re_\tau = 300$ which corresponds to a Reynolds number $Re \approx 4500$ (based on centerline properties).

With the present framework, the ablation process is mainly influenced by two parameters: the injection velocity with which one decides to initialize the computation, and the oxidation scheme retained to model the heterogeneous reactions at the wall. The set of DNS presented in this study integrates these two parameters as shown in Table 1. In this table, the initial injection velocity of reference, V_{inj}^{ref}, when expressed in wall units (scaling by $u_\tau = \sqrt{\overline{\tau_w}/\overline{\rho_w}}$) is about $V_{inj}^{+} = 0.003$ which is typical of the ablation of C/C nozzles. The two oxidation reactions of reference are the following ones:

$$C_{(s)} + H_2O \rightarrow H_2 + CO \tag{4}$$

$$C_{(s)} + CO_2 \rightarrow 2\,CO \tag{5}$$

Table 1: Description of the simulations with respect to normal injection velocity and the number of oxidation reactions. Inert case is presented in Cabrit and Nicoud, 2009.

case	V_{inj}^0/V_{inj}^{ref}	number of oxidation reactions
inert	0	0
A	1	1
B	1	2
C	4	1

for which the rate constant, K, is a relation depending on the initial molar concentrations of oxidizing species at the wall, $[X_k]_w^0$, and the initial injection velocity one wants to impose (Cabrit *et al.*, 2007). When only the first reaction is activated, $K = \rho_w V_{inj}^0 / W_C [X_{H_2O}]_w^0$. When two reactions are considered, one supposes that they have the same rate constant defined has $K = \rho_w V_{inj}^0 / W_C ([X_{H_2O}]_w^0 + [X_{CO_2}]_w^0)$.

Hence, the inert case will be used as a reference case to study the global changes induced by wall ablation. This configuration has been preliminary studied to understand the particular features of such reacting compressible TBL and results are detailed in Cabrit and Nicoud, 2009. Case A will be the reference case for ablative wall simulations because it integrates the effects of the reference initial injection velocity and of the first oxidation reaction (oxidation of solid carbon by H_2O species). Since case B integrates the second oxidation reaction (oxidation by CO_2 species), it will be compared to case A for studying the influence of the oxidation scheme. Finally, case C will be confronted to case A for investigating the initial Stephan velocity influence.

STATISTICAL PROCEDURE

The DNS's with ablative walls are statistically unsteady because the oxidation reaction at the wall consumes the H_2O species initially present in the computational domain(as well as CO_2 species when the second oxidation reaction is considered). Thus, the data cannot be averaged over time which, given the moderate size of the computational domain, makes the statistical convergence more challenging. Moreover, the time advancement of the DNS is dependent on the initial condition. For these reasons, we have performed an ensemble average from twenty different DNS's with ablative walls, differing because of the initial conditions. To insure sufficient decorrelation between the initial solutions, they are chosen from the inert wall simulation with a separating time equal to the diffusion time, $\tau_d = h/u_\tau$. The statistics convergence with this procedure is illustrated in Figure 2.

One notably observes in figure 2-a) that because of wall ablation, the mass increases linearly during the simulation. Hence, the procedure used to analyze the results and deduce information relevant to a generic TBL with ablation should be defined carefully. Indeed, the main difference between the simulated and the real cases is that the oxidizing species are continuously consumed in the simulated case (which means that no ablation would be observed for an infinite simulated time) whereas in the real case the combustion products passing through the nozzle continuously bring oxidizing species that feed the oxidation mechanism. This implies to find the appropriate scalings of the different observed variables to render them time independent. For instance, Figure 2-b) illustrates that the statistics cannot be performed before $\tau_s = \tau_d$ which is the necessary time for the flow to adapt from the initial condition. For $\tau_s > \tau_d$, the

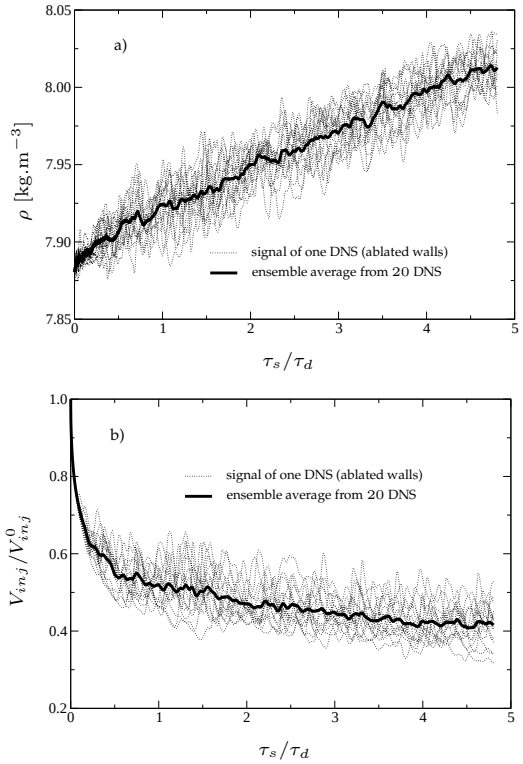

Figure 2: Evolution of the density (a) and of the injection velocity (b) for one probe situated at the wall during a typical ablative wall simulation. The velocity is scaled by the initial injection velocity, V^0_{inj}, and the simulated time, τ_s, is scaled by τ_d.

oxidation mechanism is mainly led by the diffusion of oxidizing species towards the wall and unsteady terms tend to constant values which facilitates the research of auto-similar (in time) behavior of the TBL. However, the characteristic convergence time can differ when looking at other properties than species conservation. For instance, investigating a proper method to scale the heat fluxes by the total wall heat flux, we have shown in a previous work (Cabrit and Nicoud, 2008) that convergence is reached for $\tau_s > 5\tau_d$ (this is illustrated in figure 6 that will be fully commented in the section concerning energy conservation). For this reason, the statistics presented herein are performed at a simulated time $\tau_s = 5\tau_d$. This criterion insures a good convergence of the statistics for any variable of interest in the present study.

Let us introduce the notations used in the forthcoming sections: for a variable f, $\overline{f}$ will represent the ensemble average; $\widetilde{f}$ the Favre average defined as $\widetilde{f} = \overline{\rho f}/\overline{\rho}$; the double prime, $''$, represent the turbulent fluctuations with respect to Favre averages.

RESULTS

Species conservation analysis

We have shown in our previous study (Cabrit and Nicoud, 2008) that scaling the species mass fraction profiles by their centerline value was an appropriate procedure to analyze species conservation. This is done in figure 3 where the mass fraction profiles of the oxidizing species CO_2 are presented. One first sees in this plot that the mean flow is at chemical equilibrium states in all cases (the equilibrium state has been computed *a priori* thanks to CHEMKIN software specifying the local mean concentrations and temperature). One recalls that this behavior is not numerically imposed by the code since one makes use of a seven chemical reaction mechanism to describe the flow chemical kinetics. This result is also valid for the other species (not shown herein), which means that the characteristic chemical time scale is negligible compared to the turbulent time scale (i.e. the Damköhler number is high) in the present simulations.

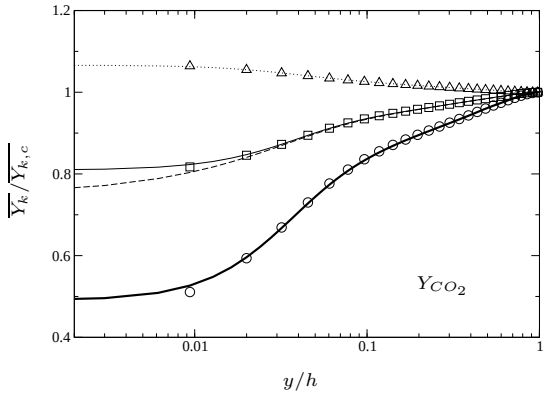

Figure 3: Mean mass fraction profile of CO_2 species scaled by its centerline value, $\overline{Y_{k,c}}$. Lines represent the DNS results, symbols the equilibrium state computed with CHEMKIN software. The same symbol is used for case A and B because their equilibrium state is identical. (····· , △): inert case; (——— , □): case A; (– – – – , □): case B; (▬▬ , ○): case C.

Comparing inert and ablative cases, one also observes that the heterogeneous reactions drastically change the species concentration profiles because of the species consummation/production features of the ablation process: the more oxidation reactions are intense, the more concentration profiles deviate from the inert wall reference case. This is visible in case C for which the injection velocity is stronger. Note that the difference between case A and B are negligible in our simulations. This is mainly due to the fact that the molar concentration of CO_2 species at the wall is one order of magnitude less than the one of H_2O. As a consequence, the second oxidation reaction slightly modify the species conservation process. Of course one cannot generalize this result since the concentration of oxidizing species at the wall directly depends on the initial concentration delivered by the initial condition. Within the present framework, this means that the only way to control the species concentration at the wall is to perform another inert simulation changing the operating conditions, and/or the species composition with which one initializes the computation.

Momentum conservation balance

Applying the ensemble average on the momentum conservation balance in the streamwise direction, and conserving the wall normal and time derivatives only, one can write:

$$\frac{d}{dy}\underbrace{\left(\tau_{\rm lam}+\tau_{\rm tur}+\tau_{\rm conv}\right)}_{\tau_{\rm tot}} = \overline{\mathcal{S}} + \frac{\partial \overline{\rho}\widetilde{u}}{\partial t} \qquad (6)$$

where $\tau_{\rm lam}$ is the laminar viscous shear stress, $\tau_{\rm tur}$ the turbulent shear, $\tau_{\rm conv}$ the convective shear, $\tau_{\rm tot}$ the total shear, and $\overline{\mathcal{S}} = \partial\overline{p}/\partial x$ the mean source term that compensates for the streamwise pressure gradient vanishing in periodic chan-

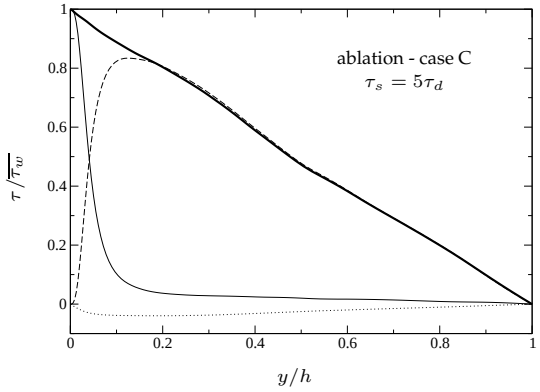

Figure 4: Momentum balance scaled by the mean total shear stress at the wall, $\overline{\tau_w}$. ——— : laminar stress, $\tau_{\rm lam} = \overline{\mu \frac{du}{dy}}$; - - - - : turbulent stress, $\tau_{\rm tur} = -\overline{\rho}\,\widetilde{u''v''}$; ····· : convective stress, $\tau_{\rm conv} = -\overline{\rho}\,\widetilde{u}\,\widetilde{v}$; ▬▬ : total shear stress, $\tau_{\rm tot}$.

nel flow configurations. Since case C is the most constraining simulation regarding to momentum conservation, it has been retained to illustrate the momentum conservation in figure 4. Because the source term is constant in space, the -1 slope of the total shear stress shows that the unsteady term of Eq. (6) is also a space constant. This indicates that the time convergence is verified for this balance. This unsteady term is less than 1% of the source term for all the DNS's, and thus negligible in the balance. Moreover, one observes that the convective term introduced by the ablation process (namely $-\overline{\rho}\widetilde{u}\widetilde{v}$) keeps small values. Indeed, the mass flux ratio $F = \overline{\rho_w\, V_{inj}}/\rho_b u_b$ (b-subscripted variables refer to bulk values) of the current simulations is too low compared to classical blowing surface studies (Simpson, 1970) to change the shear stress conservation balance: $F \approx 0.01\%$ for cases A and B, $F \approx 0.02\%$ for case C. The convective term is thus negligible, leading to the same shear stress conservation mechanism for both inert and ablative wall TBL.

Energy conservation balance

Neglecting the power of pressure forces and the viscous effect (Cabrit and Nicoud, 2009), the same analysis procedure is applied to the specific enthalpy conservation equation and leads to:

$$\frac{d}{dy}\underbrace{\left(q_{h_s} + q_{h_c} + q_{\rm Fourier} + q_{\rm spec}\right)}_{q_{\rm tot}} = \overline{\mathcal{Q}} + \frac{\partial\left(\overline{p} - \overline{\rho}\widetilde{h}\right)}{\partial t} \qquad (7)$$

where q_{h_s} is the heat flux of sensible enthalpy, q_{h_c} the heat flux of chemical enthalpy, $q_{\rm Fourier}$ the Fourier heat flux, $q_{\rm spec}$ the heat flux of species diffusion, $\overline{\mathcal{Q}}$ the space constant enthalpy source term that warms the fluid to sustain the mean temperature, and h the specific enthalpy (sum of sensible en chemical enthalpies). Figure 5 presents each term of the total heat flux balance for the inert wall case, and for ablative wall cases B and C at $\tau_s = 5\tau_d$. The total heat flux is linear through the boundary layer indicating that the unsteady term of Eq.(7) is a space constant at this time of observation (one recalls that this term is null for the inert DNS). Comparing inert and ablation cases, strong differences are visible notably because of the blowing effect of the ablation process. Indeed, for inert walls the no-slip boundary condition at the wall combined with the continuity equation imposes that $\widetilde{v} = 0$ ($\widetilde{v}$ being the Favre average wall normal

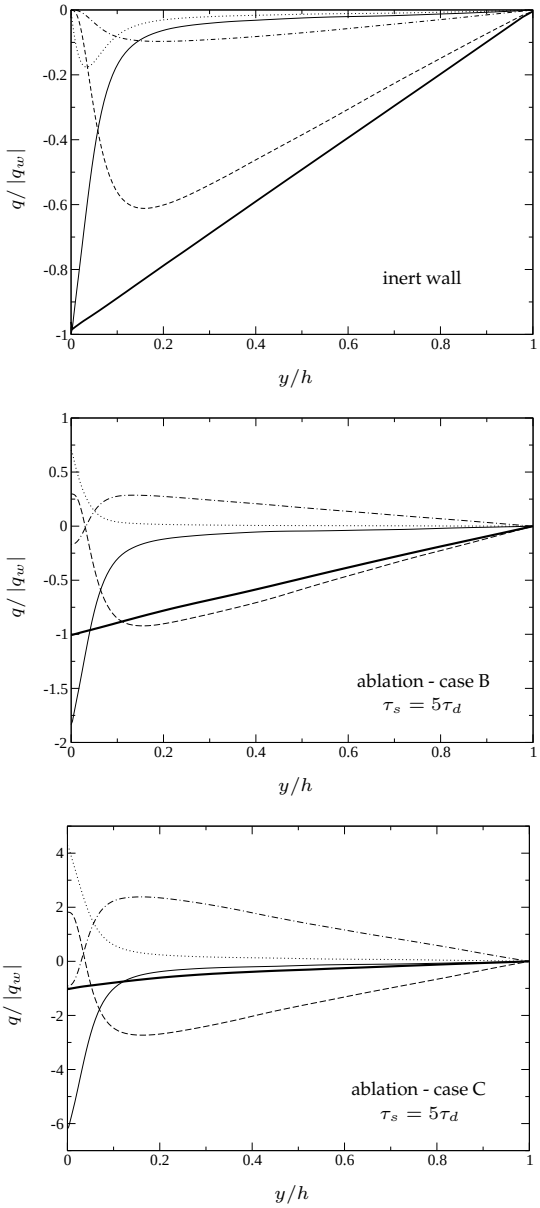

Figure 5: Heat flux balance scaled by the modulus of the flux at the wall $|q_w|$ (case A is not presented since it is very similar to case B). - - - - : flux of sensible enthalpy, $q_{h_s} = \overline{\rho}\,(\widetilde{v''h''_s} + \widetilde{v}\widetilde{h_s})$; —·— : flux of chemical enthalpy, $q_{h_c} = \overline{\rho}\sum_k(\widetilde{v''Y''_k} + \widetilde{v}\widetilde{Y_k})\Delta h^0_{f,k}$; ——— : Fourier heat flux, $q_{\rm Fourier} = -\overline{\lambda\frac{dT}{dy}}$; ····· : species diffusion flux, $q_{\rm spec} = \overline{\rho}\sum_k\{h_k Y_k V_{k,y}\}$, ($\{h_k Y_k V_{k,y}\}$ is a Favre average quantity); ▬▬ : total heat flux, $q_{\rm tot}$.

velocity). This is not the case for the ablative wall DNS. In addition, the diffusion velocities are not null at the ablative wall. As a consequence, none of the terms of the heat flux balance are null (neither negligible) at the ablative wall whereas the Fourier heat flux is the only contribution in the inert case.

Note that the changes induced by the heterogeneous reactions are not as important on the shear stress conservation since the convective term arising in the momentum balance is null at the wall (because of the null wall tangential velocity). Hence, one can postulate that for low wall normal injection velocity, the shear stress conservation process is

Table 2: Decomposition of the mean total wall heat flux. Results are scaled by the modulus of the mean total wall heat flux, $|\overline{q_w}|$.

case	$q_{h_s}/\,\lvert\overline{q_w}\rvert$	$q_{h_c}/\,\lvert\overline{q_w}\rvert$	$q_{\text{spec}}/\,\lvert\overline{q_w}\rvert$	$q_{\text{Fourier}}/\,\lvert\overline{q_w}\rvert$
inert	0%	0%	0%	-100%
A	29.2%	-16.5%	68.1%	-180.8%
B	29.8%	-16.8%	70.4%	-183.4%
C	181.9%	-90.6%	429.2%	-620.3%

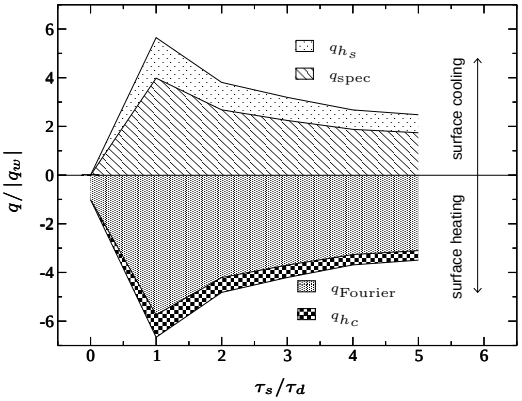

Figure 6: Typical time evolution of the heat fluxes at the wall during the ablative wall simulation.

Table 3: Comparison of the total wall heat flux for the three ablative wall cases. Results are scaled by the mean total heat flux of the inert simulation, q_w^{inert}.

case	$q_w^{\text{case}}/q_w^{\text{inert}}$
A	56%
B	55%
C	13%

not as changed as the heat flux conservation one. For the present simulations, this implies that we should mainly focus on the changes induced on heat fluxes conservation for improving the understanding of TBL with wall ablation.

Comparing cases B and C, one observes that the repartition of the fluxes composing the total heat flux are strongly modified depending on the injection velocity. This is also illustrated by table 2 that gives the importance of each heat flux at the wall. This table shows that a stronger injection velocity induces stronger disparities of the fluxes at the wall. A typical time evolution of the heat flux contributions is also presented in figure 6 in order to illustrate that the sensible enthalpy and multicomponent fluxes tend to cool the surface when ablation starts, whereas the Fourier and the chemical enthalpy fluxes contribute to surface heating. The wall surface is globally heated but table 3 indicates that the wall surface would receive a stronger total heat flux if heterogeneous reactions were not present. Moreover, one notices that the injection velocity directly influences the surface cooling effect of ablation since the total specific enthalpy flux has been divided by a factor 4.3 in case C, compared to case A and B.

Atom conservation balance

Finally, one can analyze the ablation process focussing on the atom conservation. Starting from the species conservation equation, multiplying it by:

$$M_{a,k} = n_{a,k}\,\frac{W_a}{W_k} \tag{8}$$

where $n_{a,k}$ represents the number of atoms a contained in one species k, summing over all the species, and applying the ensemble average, it is possible to find an expression for atomic mass fraction conservation in the turbulent boundary layer:

$$\frac{\partial}{\partial y}\left(\underbrace{-\sum_k \overline{\rho}\mathcal{D}_k M_{a,k}\frac{\partial \widetilde{Y_k}}{\partial y}}_{\phi_{\text{lam},a}} + \underbrace{\overline{\rho}\,\widetilde{v''\psi_a''}}_{\phi_{\text{tur},a}} + \underbrace{\overline{\rho}\,\widetilde{v}\,\widetilde{\psi_a}}_{\phi_{\text{conv},a}}\right) = \overline{\dot{\omega}_a} \tag{9}$$

In this expression, ψ_a stands for the atomic mass fraction of atom a, and $\overline{\dot{\omega}_a} = -\partial\overline{\rho}\widetilde{\psi_a}/\partial t$ is the source term of atom a. One recognizes a classical conservation law where $\phi_{\text{lam},a}$ is the laminar flux of atom a, $\phi_{\text{tur},a}$ the turbulent flux, and $\phi_{\text{conv},a}$ the convective flux.

Hence, the balances of atomic mass fraction fluxes has been plotted for each atom in figure 7. Only the results of case B are presented in this figure but the conclusions are similar for other ablative wall simulations. From a qualitative point of view, one can observe that the wall normal variation of the laminar and the turbulent atomic fluxes seem to be of classical type (see the shear stress balance Fig. 4 as a comparison).

Furthermore, this figure illustrates that the conservation balance of atom C is different from the other ones. The difference is due to the atomic source term which is null for atoms H, O, and N (no production or consummation of these atoms can arise in the TBL), whereas the heterogeneous reactions transform the carbon of solid surface into gaseous species composed of carbon atom. The latter process acts like a production source term of carbon atoms injected from the wall surface towards the TBL. As a consequence, one observes a -1 slope on the total carbon flux balance which is replaced by a constant value for other atoms (of course the value of this constant is zero because no flux of these atoms arise at the wall, and because any mean wall normal flux is necessary null at the centerline of such channel flows). Note that the constant slope observed for the total atomic flux of atom C is due to the fact that the balances have been performed at a converged time for which the time derivatives are constant in space.

Moreover, since the turbulent atomic flux is null at the wall, one can verify that the convective and the laminar diffusive fluxes strictly compensate each other at the wall surface for atoms H, O, and N. Indeed, the heterogeneous reaction mechanism is fed by laminar atomic fluxes, and delivers a convective atomic flux towards the TBL. Regarding to carbon atom, one understands that this mechanism is superposed to a convective mechanism ejecting carbon atoms taken from the solid surface towards the TBL. The resulting total carbon flux at the wall thus characterizes the solid surface recession.

CONCLUSION

This study presents a generic method for performing DNS's of periodic channel flow with ablative walls. The analysis of the generated data is made easier if the time dependancy can be neglected, which appears to be the case in the present study after a few diffusion times. Making use

of ensemble averages to improve the statistical convergence, some particular features of ablative wall TBL have been analyzed such as the chemical equilibrium of the mixture, the effect of the injection velocity on the shear stress and heat flux balances, and the surface cooling effect of wall ablation. Finally, we have derived an atomic mass fraction conservation equation that can be used to analyze the atomic fluxes in terms of laminar, turbulent and convective contributions.

The authors gratefully acknowledge the CINES for the access to supercomputer facilities, and want to thank the support and expertise of Snecma Propulsion Solide.

REFERENCES

J. Zhong, T. Ozawa, and D. A. Levin, 2008. "Modeling of stardust reentry ablation flows in near-continuum flight regime." *AIAA J.*, 46(10):2568–2581.

J. H. Koo, D. W. H. Ho, and O. A. Ezekoye, 2006. "A review of numerical and experimental characterization of thermal protection materials - part I. numerical modeling." n *42nd AIAA/ASME/SAE/ASEE Joint Propulsion Conference and Exhibit*, Sacramento, California, 9-12 July 2006.

S. T. Keswani and K. K. Kuo, 1983. "An aerothermochemical model of carbon-carbon composite nozzle recession." *AIAA Paper 83-910.*

P. Baiocco and P. Bellomi, 1996. "A coupled thermo-ablative and fluid dynamic analysis for numerical application to solid propellant rockets." *AIAA Paper 96-1811.*

R. M. Kendall, R. A. Rindal, and E. P. Bartlett, 1967. "A multicomponent boundary layer chemically coupled to an ablating surface." *AIAA Journal*, 5(6):1063–1071.

O. Cabrit, L. Artal, and F. Nicoud, 2007. "Direct numerical simulation of turbulent multispecies channel flow with wall ablation." *AIAA Paper 2007-4401*, 39th AIAA Thermophysics Conference, 25-28 June.

P. Schmitt, T. Poinsot, B. Schuermans, and K. P. Geigle, 2007. "Large-eddy simulation and experimental study of heat transfer, nitric oxide emissions and combustion instability in a swirled turbulent high-pressure burner." *J. Fluid Mech.*, 570:17–46.

S. Mendez and F. Nicoud, 2008. "Large-eddy simulation of a bi-periodic turbulent flow with effusion." *J. Fluid Mech.*, 598:27–65.

J. Kim, P. Moin, and R. Moser, 1987. "Turbulence statistics in fully developed channel flow at low Reynolds number." *J. Fluid Mech.*, 177:133–166.

J.O. Hirschfelder, F. Curtiss, and R.B. Bird, 1964. *Molecular theory of gases and liquids.* John Wiley & Sons.

Y. Sumitani and N. Kasagi, 1995. "Direct numerical simulation of turbulent transport with uniform wall injection and suction." *AIAA J.*, 33(7):1220–1228.

O. Cabrit and F. Nicoud, 2009. "Direct simulations for wall modeling of multicomponent reacting compressible turbulent flows." *accepted in Phys. Fluids.*

O. Cabrit and F. Nicoud, 2008. "DNS of a periodic channel flow with isothermal ablative wall." In *ERCOFTAC workshop - DLES 7*, Trieste, Italy, 8-10 September 2008.

R. L. Simpson, 1970. "Characteristics of turbulent boundary layers at low Reynolds numbers with and without transpiration." *J. Fluid Mech.*, 42(4):769–802.

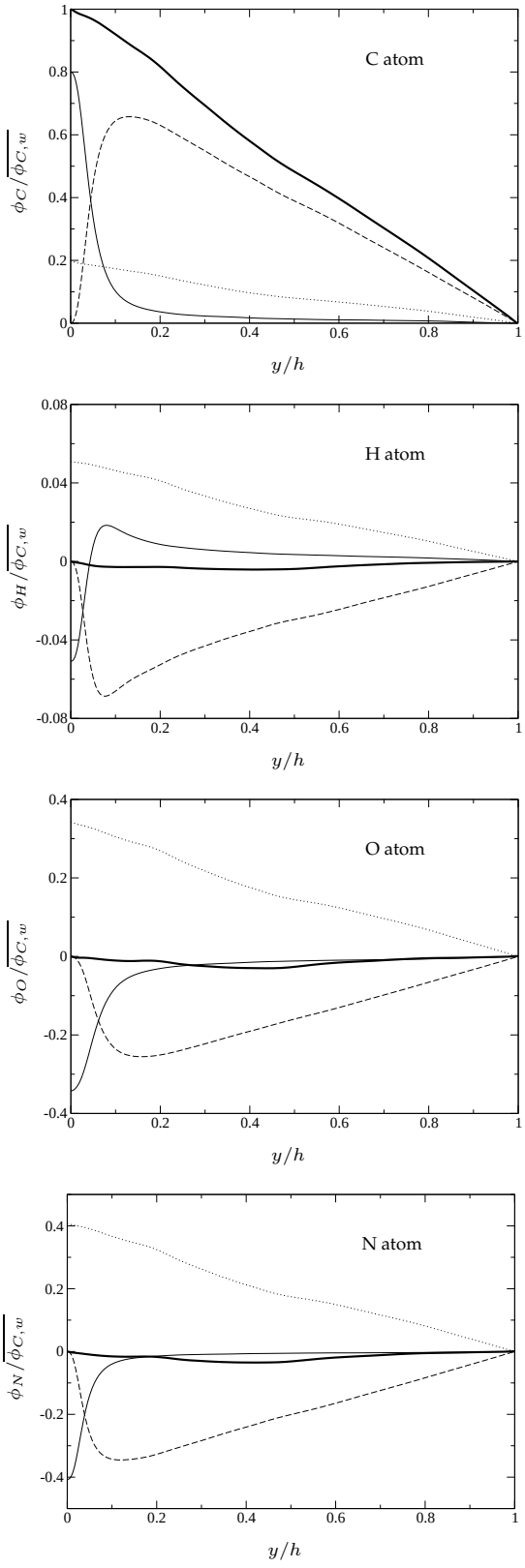

Figure 7: Atomic flux balance for case B. Fluxes are scaled by the mean total atomic mass fraction flux of carbon atom at the wall $\overline{\phi_{C,w}}$. ——— : laminar flux, $\phi_{\mathrm{lam},a}$; – – – – : turbulent flux, $\phi_{\mathrm{tur},a}$; ····· : convective flux, $\phi_{\mathrm{conv},a}$; ▬▬▬ : total atomic flux, $\phi_{\mathrm{tot},a} = \phi_{\mathrm{lam},a} + \phi_{\mathrm{tur},a} + \phi_{\mathrm{conv},a}$.